THE JOURNAL OF PHYSICAL CHEMISTRY B

ARTICLE

pubs.acs.org/JPCB

Role of Anionic Micellar Template on the Morphology, Solid-State Ordering, and Unusual Conductivity Trend in Poly(aniline-*co*-pyrrole) Nanomaterials

M. Jinish Antony[†] and M. Jayakannan[*,‡]

[†]Chemical Sciences and Technology Division, National Institute for Interdisciplinary Science and Technology, Thiruvananthapuram 695019, Kerala, India

[‡]Department of Chemistry, Indian Institute of Science Education and Research (IISER), 900, NCL Innovation Park, Dr. Homi Bhabha Road, Pune-411 008, Maharashtra, India

Supporting Information

ABSTRACT: Here, we report three structurally different anionic amphiphilic dopant micellar templates for the development of poly(aniline-*co*-pyrrole) copolymer nanomaterials and investigating the role of dopant on the morphology, solid-state ordering, and unusual bulk conductivity trend in conducting nanostructures. All three amphiphilic dopants possessed identical azobenzene sulfonic acid as polar head but vary in their hydrophobic alkyl tails. Dynamic light scattering analysis confirmed the formation of 4.3 and 100 nm micelles by the single tail and double tail amphiphiles in water, respectively. Upon adding aniline or pyrrole (or mixture of both), the dopant micelles produce a thick white emulsion containing micrometer size larger aggregates, which template for nanomaterial. The copolymer nanomaterials were synthesized by varying the amount of aniline and pyrrole in the feed from 0 to 100 mol % under identical emulsion polymerization routes. Electron microscopic analysis (SEM and TEM) revealed that the morphology of the copolymer nanomaterials transformed from nanofiber to nanospheres via nanorods upon increasing the composition of pyrrole in the feed. Four probe bulk conductivities of the nanomaterials, which were produced on the basis of single tail dopant (or no tail dopant), showed unusual nonlinear trend over the pyrrole composition. Because all three copolymers series showed similar morphology evolution, the influence of morphology transformation on the unusual trend in the bulk conductivities was ruled out. The percent crystallinity of the samples obtained from WXRD spectra provides direct evidence that the bulk conductivity of the copolymer conducting nanomaterials is primarily influenced by their three-dimensional solid-state ordering rather than other factors such as morphology transformation. The structure of the dopant plays major roles in arranging the polymer−dopant complexes in highly ordered forms, which contribute to their bulk conductivity behaviors in the solid state.

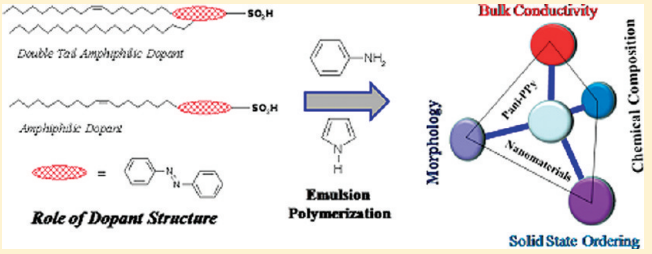

INTRODUCTION

Conducting polymer nanomaterials possessing one-dimensional nanostructure were extensively used in chemical-electrochemical-bio sensors, optoelectronic devices, solid-state electrolytes, hydrogen storage, and so on.[1−5] Polyaniline (PANI) and polypyrrole (PPy) are very important conducting polymers. Control of size and shape of these conducting structures in nanosize level has been realized as an important task to obtain superior surface and electron transport properties in devices.[6−10] Synthesis of conducting polymer nanomaterials was typically achieved using hard templates approaches like anodic alumina, porous silica, electrospinning methods, and also by soft template approaches like amphiphilic dopant acids, gels, lipids, liquid crystals, etc.[11−22] Among various soft templates, the surfactant micelle approach attained wide interest due to the formation of predictable size and shape of nanomaterials. Both cationic and anionic dopants were employed to produce conducting polymer nanomaterials; however, the removal of cationic and nonionic dopants during the purification step induces instability and insolubility of nanomaterials.[11−13] On the other hand, anionic dopants act as dopant-cum-template and stabilize the polymer matrix via electrostatic interaction.[23−29] The electrostatic binding of the long chain dopant permanently at the nanostrcutures improves the solubility, colloidal stability, conductivity, and solid-state packing of the nanomaterials. It is rather surprising to note that anionic dopants exclusively template for polyaniline and their cationic counterpart for polypyrrole nanomaterials. Almost there are no dopants available based on either anionic or cationic, which could be employed as template for both aniline and pyrrole under identical polymerization conditions. The requirement of such common surfactant-cum-dopant for both aniline and pyrrole is very crucial because the approach could be

Received: February 17, 2011
Revised: April 19, 2011
Published: May 03, 2011

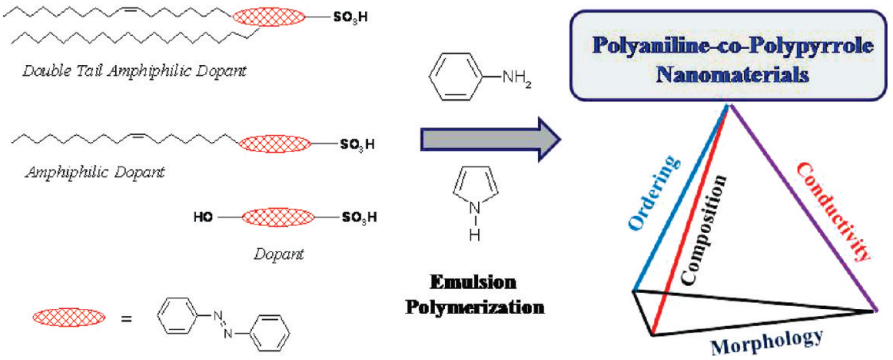

Figure 1. Schematic representation of the role of anionic amphiphilic dopants on the properties of copolymer nanomaterials.

extended to make new poly(aniline-*co*-pyrrole) copolymer nanomaterials. To address the above issue, recently, we have developed a new emulsion-mediated process based on amphiphilic azobenzene sulfonic acid. The azobenzene-based dopants are very unique in the sense that it exclusively produced polyaniline nanofibers and polypyrrole nanospheres under the identical experimental conditions.[30,31] The preliminary attempts to utilize the micellar medium for both aniline and pyrrole revealed that the resultant copolymer nanomaterials showed morphology transformation and unusual conductivity behaviors.[31b,c] Although the poly(aniline-*co*-pyrrole) copolymers were successfully produced by the azobenzene dopant, it was rather difficult to establish the correlation between the structural characteristics of the dopant with the unusual conductivity behaviors of the copolymers. Further, the copolymers were found amorphous unlike their crystalline homopolymers, which also restricted the understanding of the role of solid-state ordering on the conductivity behaviors. Therefore, new dopant molecular designs are required to understand the unusual conductivity behavior of the poly(aniline-*co*-pyrrole). Stejskal et al. and Lim et al. separately reported a nonlinear trend in the conductivity of poly(aniline-*co*-pyrrole) samples doped by HCl (not nanomaterials).[32,33] Despite the fact that significant efforts had been paid to understand the polyaniline and polypyrrole nanostructures, the unusual conductivity and morphological features of their copolymer nanomaterials are still unresolved.[34−38] Typically, four important parameters like solid-state ordering, dopant structure and chemical composition, morphology, and conductivity influence the pyramidal characteristic of conducting nanomaterials in the solid state (see Figure 1). The large discrepancy in the literature reports on how the properties of homopolymers caused difficulties in correlation with the bulk conductivities of the copolymer nanomaterials. Therefore, it is very important to develop a unique molecular template approach for poly(aniline-*co*-pyrrole) copolymer nanomaterials to establish their various structure−property relationships with conductivity such as (i) role of structure of the dopant, (ii) role of morphologies, (iii) influence of solid-state ordering, and (iv) monomer composition in the copolymer. These points are very important and crucial in the conducting polymer nanomaterials research because the copolymer materials may possess unique properties and provide new applications, which are not characteristic for corresponding homopolymers.

The present investigation addresses the above issues by carefully choosing three structurally different anionic dopants, which were designed, synthesized, and employed as templates for poly(aniline-*co*-pyrrole) nanomaterials (see Figure 1). The polar headgroup is fixed as azobenzene sulfonic acid unit in all three dopants, and their nonpolar tail nature is varied via tailor-made approaches. The surfantant-1 has a single tail with C15-alkyl chain having an unsaturated double bond. Dopant-2 carries a double tail, each one corresponding to C15-unsaturated and C12-saturated chains. The third dopant-3 has only hydrophilic head and no tail attached. The nanomaterials were synthesized by the emulsion polymerization route at ambient conditions. The compositions of the monomers in the feed varied from 0 to 100% of pyrrole. The nanomaterials were characterized by SEM, TEM, WXRD, NMR, FT-IR, and UV−visible spectroscopy and four-probe conductivity measurements, etc. The copolymer nanomaterials were found to show nanofiber, nanorod, and nanosphere morphology. The nature of the dopant and solid-state ordering were found to play major roles in the nonlinear conductivity behaviors of the samples with respect to their composition. In short, the present investigation provides direct correlation between the morphology, electronic, and solid-state properties with the nonlinear trend in the poly(aniline-*co*-pyrrole) copolymers nanomaterial, which is achieved through carefully designed structurally different amphiphilic dopant-cum-surfactant in water.

EXPERIMENTAL SECTION

Materials. Pyrrole, aniline, ammonium persulfate (APS), dodecyl bromide, phenol, and sulfanilic acid were purchased from Sigma-Aldrich. Cardanol was purified by double-vacuum distillation at 3−4 mm of Hg, and the fraction distilled at 220−235 °C was collected. The single tail amphiphilic dopant 4-[4-hydroxy-2((*Z*)-pentadec-8-enyl)phenylazo]-benzenesulphonic acid (dopant-1) and polyaniline, polyrrole, and poly(aniline-*co*-pyrrole) copolymers based on dopant-1 were synthesized as reported earlier.[31]

Measurements. ^{1}H NMR analysis of the dopant and polymer samples were carried out on a 500 MHz Bruker Avance II NMR spectrometer in d_6-dimethyl sulphoxide (DMSO) containing a small amount of tetramethylsilane (TMS) as internal standard. Infrared spectra of the polymers were recorded using a Perkin-Elmer Spectrum One FT-IR spectrometer in the range of 4000−400 cm^{-1}. The purity of the compounds was determined by fast atom bombardment high-resolution mass spectrometry (FAB-HRMS: JEOL JSM 600). For SEM measurements, polymer samples were subjected to a thin gold coating using a JEOL JFC-1200 fine coater. The probing side was inserted into a JEOL JSM-5600 LV scanning electron microscope for taking

photographs. TEM analysis of the sample was recorded using a Tecnai 30 G^2 S-twin 300 KV high-resolution transmission electron microscope. A suspension of nanomaterials was prepared in ethanol and deposited on a Formvar-coated copper grid before TEM analysis. UV−visible spectra of the copolymers are recorded using a Perkin-Elmer Lambda-35 UV−visible spectrometer. DLS measurement was done by a Nano ZS Malvern instrument employing a 4 mW He−Ne laser (λ = 632.8 nm) and equipped with a thermostatted sample chamber. Water was used as solvent, and the measurements were carried out at 25 °C. The concentrations of the dopants used for the measurements were 1×10^{-3} M, whereas for copolymer mixtures the concentration used was 9.6×10^{-3} M. For conductivity measurements, the polymer samples were pressed into 10 mm diameter and 1 mm thickness pellet and analyzed by the four-probe method using Keithley 6221 DC and AC current source and 2181A nano voltmeter. Wide angle X-ray diffraction (WXRD) patterns of the finely powdered polymer samples were recorded by a Philips analytical diffractometer using Cu Kα emission. The spectra were recorded in the range of 2θ = 0−40° and analyzed using X'Pert software. The thermal stability of the polymers was determined using a PerkinElmer STA 6000 simultaneous thermal analyzer at a heating rate of 10 °C/min in nitrogen. The TGA instrument was calibrated with calcium oxalate monohydrate as standard.

Synthesis of 4-[4-Dodecyloxy-2((*Z*)-pentadec-8-enyl) phenylazo]-benzenesulphonic Acid (Dopant-2). Dopant-1 (5.0 g, 10.3 mmol) was added to a powdered suspension of KOH (1.1 g, 20.4 mmol) in 10 mL of dimethylsulfoxide. Dodecylbromide (3.2 g, 12.9 mmol) was added drop by drop to the above reaction mixture at 60 °C for 12 h. The sodium salt of the product was precipitated in acetone, and the solid was filtered through a suction pump. The solid was acidified using 2 M HCl, filtered, and dried in a vacuum oven. It was further purified by passing through silica gel column using 30% methanol in ethyl acetate. Yield = 3.3 g (49%). ^{1}H NMR (500 MHz, d_6-DMSO) δ: 7.76 (s, 4H, Ar−H), 7.64 (d, 1H, Ar−H), 6.90 (s, 1H, Ar−H), 6.83 (d, 1H, Ar−H), 5.24 (2H, CH═CH), 4.04 (t, 2H, −O−**CH$_2$**), 3.1−3.06 (m, 50H, aliphatic-H). ^{13}C NMR (125 MHz, d_6-DMSO) δ: 161.3, 152.2, 149.6, 145.0, 143.6, 129.7, 126.6, 121.7, 116.7, 115.0, 112.5,69.7, 68.8, 31.0, 31.24, 30.77, 29.14, 28.85, 26.9 25.4, 22.0, 13.5. FT-IR (KBr, cm^{-1}): 2923, 2854, 2852.9, 1600, 1533.7, 1472, 1397, 1338, 1228, 1136, 1016, 852, 716, 636. UV−vis (in H_2O, nm) λ_{max}: 365. FAB-MS (MW 654.99): m/z = 654.44 (M^+).

Synthesis of 4-[4-Hydroxy phenylazo]-benzene Sulfonic Acid (Dopant-3). Sulphanilic acid (11.0 g, 53.28 mmol) and sodium carbonate (2.8 g, 26.6 mmol) were added into 50 mL of water and heated to 60−70 °C to dissolve the entire solid. It was then cooled to 5 °C, and a cold solution of sodium nitrite (4.0 g, 58.5 mmol) in water (8 mL) was added. The resultant yellow solution was poured into ice (50 g) containing concentrated HCl (8 mL) and stirred using a mechanical stirrer for 30 min at 5 °C. Cold diazonium chloride solution was added dropwise into the mixture of phenol (5.0 g, 53.2 mmol) and sodium hydroxide (6.38, 159.6 mmol) in 30 mL of water at 5 °C. The reaction was continued with stirring for 3 h in the ice cold conditions using a mechanical stirrer. The reaction mixture was neutralized by the addition of concentrated HCl (50 mL) in crushed ice (70 g). The red precipitate was filtered using a Buchner funnel and washed with water. The dried product weighed 12.0 g (crude product). It was further purified by passing through a silica gel column using 50% methanol in ethyl acetate. The solvent was removed to obtain the product as a red-orange solid. Yield = 10.4 g (70%). ^{1}H NMR (500 MHz, d_6-DMSO) δ: 7.85 (d, 2H, Ar−H), 7.8 (s, 4H, Ar−H), 6.95 ppm (d, 2H, Ar−H). ^{13}C NMR (125 MHz, d_6-DMSO) δ: 161.2, 151.8, 149.74, 145.1, 126.8, 125.1, 121.4, 116.5. FT-IR (KBr, cm^{-1}): 2923, 2853, 1602, 1486, 1388, 1244, 1184, 1129, 1048, 852, 714, 639 cm^{-1}. UV−vis (in CH_3OH, nm): λ_{max} = 330. FAB-MS (MW 278): m/z = 278.28 (M^+).

Preparation of Polyaniline Nanofiber via Emulsion Route Using Dopant-2. A typical procedure for the synthesis of polyaniline nanofiber using dopant-2 is given below. Dopant-2 (94 mg, 0.144 mmol) was taken in 10 mL of water and stirred under sonication for 15 min. Aniline (1 mL, 11 mmol) was added to the dopant solution and sonicated for 45 min. At the end of stirring, the polymerization mixture turned into a pale yellow thick emulsion. Ammonium persulfate (3.3 g, 14.4 mmol) in water (5 mL) was added dropwise to the solution, and the stirring was continued under sonication for 1 h. The polymerization was continued without disturbance for 12 h at 25 °C. The sample was filtered and washed with water and methanol until the filtrate become colorless. The green nanomaterial was dried under a vacuum oven for 12 h at 50 °C. Yield = 97%. ^{1}H NMR (500 MHz, d_6-DMSO) δ: 7.40 (m, 2H, PANI), 7.44 (m, 2H, PANI), 7.78 (s, 4H, Ar−H dopant). FT-IR (KBr, cm^{-1}): 1560, 1494, 1346, 1193, 1111, 1050, 923, 811, 783, 612. UV−visible (in water, nm) λ_{max}: 350, 450, 900.

A similar procedure is adopted for the synthesis of polyaniline using dopant-3. Polypyrrole samples **PPY-1**, **PPY-2**, and **PPY-3** were synthesized using a similar procedure by adopting 1 mL of pyrrole instead of aniline.

Preparation of Poly(aniline-*co*-pyrrole) Copolymer Nanomaterials. A typical procedure for the synthesis of **P2−Co-13** is given below. Dopant-2 (94 mg, 0.144 mmol) is taken in a round-bottom tube in 10 mL of water and stirred under sonication for 15 min. Pyrrole (0.1 mL, 1.44 mmol) and aniline (0.9 mL, 9.9 mmol) are added to the dopant solution and stirred under sonication for 45 min. At the end of the stirring, the polymerization mixture turned into a pale yellow thick emulsion. Ammonium persulfate (3.28 g, 14.4 mmol) in water (5 mL) was added dropwise to the solution, and stirring was continued under sonication for 1 h. The reaction was then allowed to continue for 8 h without further disturbance at 25 °C. The sample was filtered and washed with water and methanol until the filtrate become colorless. The polypyrrole nanomaterial is dried under a vacuum oven for 12 h at 50 °C. Yield = 89%. ^{1}H NMR (500 MHz, d_6-DMSO) δ: 7.40 (m, 2H, PANI), 7.44 (m, 2H, PANI), 7.29 (d, 2H, PPY) 7.78 (s, 4H, Ar−H dopant). FT-IR (KBr, cm^{-1}): 1540, 1460, 1360, 1295, 1181, 1090, 1036, 960, 905, 783, 670, 612. UV−vis (water, nm) λ_{max}: 480 and 1000.

Copolymer **P2−Co-6**, **P2−Co-13**, **P2−Co-36**, **P2−Co-57**, **P2−Co-75**, and **P2−Co-92** were synthesized using the above procedure with various mole ratios of pyrrole and aniline (see Table 1). A similar procedure was adapted to synthesis copolymers **P3−Co-*Y*** using dopant-3. The concentration dopant, mole ratio, and elemental analysis ratio are shown in Table 1.

RESULTS AND DISCUSSION

Three amphiphilic dopants were synthesized as shown in Scheme 1. Diazotization of sulphanilic acid and electrophilic substitution of the resultant diazonium salt with cardanol and phenol produced amphiphilic dopant-cum-surfactants,

Table 1. Concentration of Monomers and Dopant, Element Analysis, Conductivity, and Size of Nanostructures

sample	conc. of pyrrole (M)	conc. of aniline (M)	water in (mL)[a]	S/N ratio[b]	σ[c] (S/cm)	size of nanostructures[d] (nm)
PANI-2	0	7.3×10^{-1}	10	0.49	0.20 ($\pm$0.01)	F, 380 $\pm$ 20
P2−Co-6	4.8×10^{-2}	6.9×10^{-1}	10	0.42	0.38 ($\pm$0.01)	R, 200 $\pm$ 20
P2−Co-13	9.6×10^{-2}	6.6×10^{-1}	10	0.34	0.42 ($\pm$0.02)	R, 200 $\pm$ 20
P2−Co-36	2.8×10^{-1}	5.1×10^{-1}	10	0.25	0.38 ($\pm$0.02)	S, 250 $\pm$ 20
P2−Co-57	4.8×10^{-1}	3.6×10^{-1}	10	0.24	0.16 ($\pm$0.01)	S, 250 $\pm$ 20
P2−Co-75	6.7×10^{-1}	2.2×10^{-1}	10	0.26	0.22 ($\pm$0.03)	S, 230 $\pm$ 20
P2−Co-92	8.6×10^{-1}	7.3×10^{-2}	10	0.26	0.34 ($\pm$0.04)	S, 280 $\pm$ 20
PANI-3	0	7.3×10^{-1}	10	0.44	2.3×10^{-3} ($\pm 1 \times 10^{-4}$)	F, 50 $\pm$ 20
P3−Co-6	4.8×10^{-2}	6.9×10^{-1}	10	0.40	$2.6 \times 10^{-3} \pm (1.5 \times 10^{-4})$	R, 50 $\pm$ 20
P3−Co-13	9.6×10^{-2}	6.6×10^{-1}	10	0.39	$9.4 \times 10^{-3} \pm (3 \times 10^{-4})$	R, 50 $\pm$ 20
P3−Co-36	2.8×10^{-1}	5.1×10^{-1}	10	0.28	$5.6 \times 10^{-5} \pm (1 \times 10^{-5})$	S, 200 $\pm$ 20
P3−Co-57	4.8×10^{-1}	3.6×10^{-1}	10	0.23	$3.0 \times 10^{-4} \pm (1.5 \times 10^{-4})$	S, 200 $\pm$ 20

[a] Ammonium persulfate (14.4 mmol) in 5 mL of water was added to the polymerization mixture containing monomers (aniline + pyrrole) and dopant concentration 9.6×10^{-3} M in water. [b] S/N ratio of the copolymer nanomaterial calculated from elemental analysis. [c] Conductivity of the copolymer nanomaterials measured using four probe conductivity meter at 30 °C. [d] Width or diameter of the nanostructures such as fiber (F), rod (R), and sphere (S).

Scheme 1. Synthesis of Amphiphilic Dopants

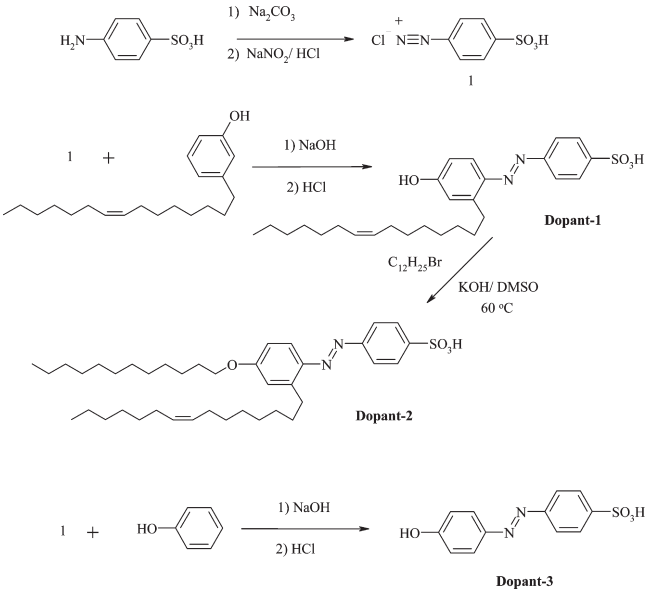

4-[4-hydroxy-2((*Z*)-pentadec-8-enyl) phenylazo]-benzenesulphonic acid (dopant-1) and 4-[4-hydroxy phenylazo]-benzenesulphonic acid (dopant-3), respectively. Cardanol is a naturally occurring phenol obtained from the cashew nut liquid (CNSL) oil, an industrial byproduct from the cashew nut processing industry. Dopant-1 was subjected to a nucleophilic substitution reaction with dodecyl bromide to produce a double-tailed dopant 4-[4-dodecyloxy-2((*Z*)-pentadec-8-enyl) phenylazo]-benzenesulphonic acid (dopant-2). Cardanol-based dopants have a unique built-in amphiphilic design in which the hydrophilic sulfonic acid behaves as a polar head and the long alkyl chain as a hydrophobic tail. Dopant-3 possessed only azobenzene sulfonic acid headgroup without any tail. The main structural difference of the dopants arose from their difference in their hydrophobic tail part, but all bear identical hydrophilic heads. The purity and structure formation of the dopants were confirmed by NMR, FT-IR, and HR-MS (see the Supporting Information). ^{1}H NMR spectra of all three surfactant-cum dopants were shown in Figure 2. Dopant-1 has a peak at 7.80 ppm with respect to four protons in the aromatic ring of Ar−SO_3H and two doublets at 7.65 ppm, 6.80 ppm and one singlet at 6.75 ppm with respect to the Ar−OH ring. The HC═CH protons appeared at 5.27 ppm, confirming the unsaturated nature of the alkyl chain. Dopant-2 was synthesized from dopant-1, and it has all aromatic protons similar to that of dopant-1; however, a new peak appeared at 4.02 with respect to Ar−O−**CH_2**− protons as a result of alkylation at the Ar−OH. ^{1}H NMR spectra of dopant-3 showed a peak at 7.80 corresponding to the aromatic ring Ar−SO_3H and two doublets at 7.85 and 6.95 ppm with respect to Ar−OH. ^{13}C NMR spectra and FAB-mass of the samples also confirmed the structure of the dopants (see the Supporting Information). To trace the micellar behavior of the dopants, they were subjected to dynamic light scattering analysis in water. DLS histograms of dopant-1 and dopant-2 are shown in Figure 3. Dopant-1 forms tiny micelles of 4.3 nm diameter in water, whereas the size of the micelles in dopant-2 was obtained as 100 nm. The formation of large size micelles in dopant-2 was attributed to the presence of the double hydrophobic tail. Dopant-3 did not show formation of any specific aggregates. Upon adding aniline or pyrrole or aniline+pyrrole mixture, the clear dopant micellar solution turned into a thick white emulsion. The DLS histograms of the emulsion corresponding to the copolymer mixtures are shown along with the dopants in Figure 3. The polymerization mixtures were found as larger aggregates of 0.8−1.0 μm in size. The formation of larger aggregates could be explained on the basis of the interaction of the acidic dopant micelles with the basic aromatic molecules such as aniline and pyrrole. The sizes of the aggregates were almost identical for aniline+dopant, pyrrole+dopant, and all of the copolymer compositions (see the Supporting Information). This suggests that the dopant micelles are very versatile to form micrometer size stable polymerization aggregated templates with both aniline and pyrrole and their mixtures. Subsequently, these emulsion mixtures were polymerized by adding an aqueous solution of ammonium persulphate in ice cold condition and keeping the reaction mixture without disturbance overnight. The resultant dark green material was filtered and washed with water

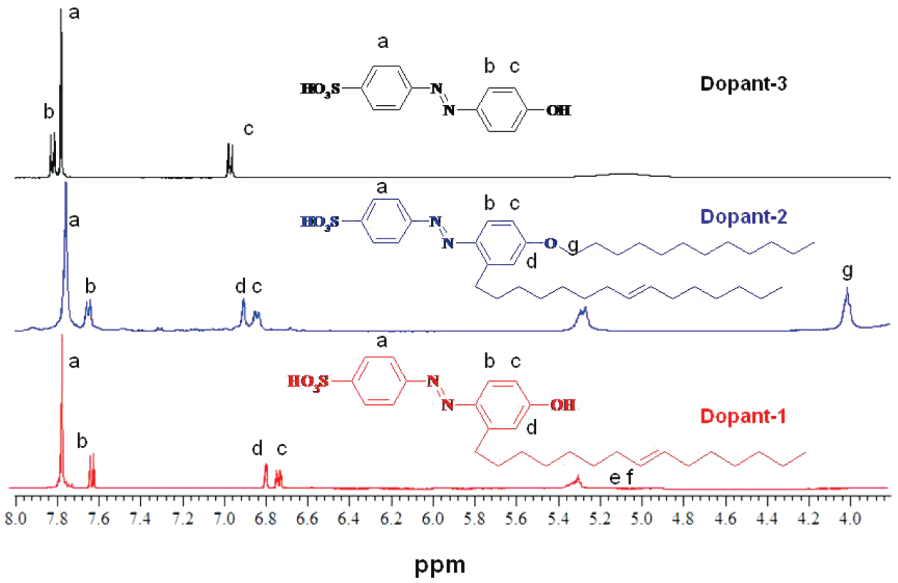

Figure 2. ^{1}H NMR spectra of dopant-1, dopant-2, and dopant-3. Spectra are expanded from 8 to 3.5 ppm for better clarity.

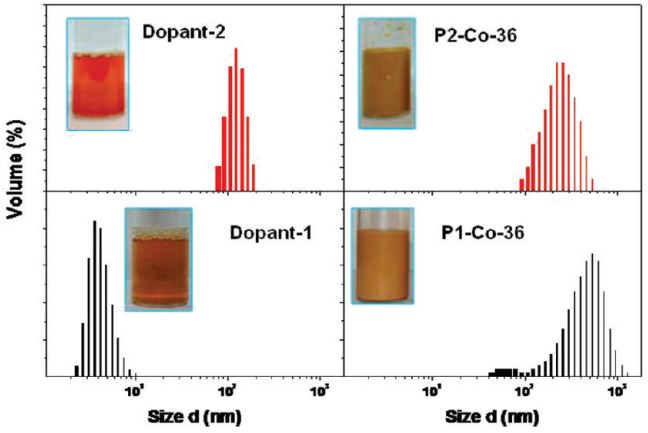

Figure 3. DLS histograms of dopant-1, dopant-2, and the emulsions corresponding to the copolymer mixtures **P1−Co-36** and **P2−Co-36**.

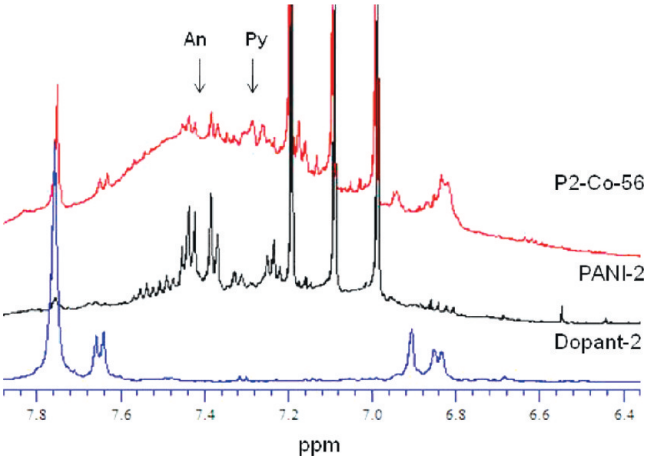

Figure 4. ^{1}H NMR spectra of dopant-2, **PANI-2**, and copolymer **P2−Co-56**. Spectra are expanded from 8 to 6.4 ppm for better clarity.

and methanol until the filtrate became colorless. It was dried under a vacuum oven for 24 h (0.05 mm of Hg) at 50 °C prior to further analysis. Unfortunately, the emulsion produced by dopant-3 was not very stable for DLS measurements. Additionally, in the case of the dopant-3 series, at higher pyrrole amount in the copolymerization mixture either oil formation or precipitation was noticed, which restricted the variation of composition to more than 60% of pyrrole. The copolymers are denoted as **P*X*−Co-*Y***, where ***Y*** is the mole % of pyrrole used for copolymer synthesis in feed, whereas $X = 1$, 2, and 3 for dopant-1, dopant-2, and dopant-3, respectively. Homopolymer nanomaterials polyaniline (**PANI-*X***) and polypyrrole (**PPy-*X***) were synthesized by polymerizing either aniline or pyrrole with dopants under identical conditions.

In general, poly(aniline-*co*-pyrrole) copolymers were insoluble in nature due to the rigid polymer chains; however, in the present case, the long alkyl chains of the amphiphilic dopant enhance the solubility of the nanomaterials for structural characterization. Dopant-3 does not have alkyl chains, and the polymer samples prepared by dopant-3 were insoluble, which restrict their characterization by NMR. ^{1}H NMR spectra of the copolymers synthesized using dopant-2 are shown in Figure 4 (for other series of dopant-1, please see the Supporting Information). **PANI-2** showed two aromatic protons at 7.45 and 7.40 ppm with respect to the aromatic protons in the polyaniline chains. Copolymer **P2−Co-56** showed a peak at 7.29 ppm corresponding to β-protons in pyrrole in addition to the polyaniline protons.[39] ^{1}H NMR spectra are clearly evident for the incorporation of the aniline and pyrrole units in the copolymer nanomaterials; however, based on NMR spectra, in the present case, it is very difficult to differentiate whether the polymer samples are interpenetrating of two homopolymers or random copolymers. For this purpose, FT-IR spectra of the copolymers were recorded by making samples into a thin pellet with KBr (see Figure 5 in the Supporting Information). The peaks are assigned with appropriate band structures (A = aniline and P = pyrrole). The polyaniline (**PANI**) has two peaks at 1580 and 1490 cm^{-1} with respect to the stretching vibration of quinoid and benzenoid in polyaniline chains, respectively.[30,31,40] Three additional peaks

dx.doi.org/10.1021/jp2015726 |*J. Phys. Chem. B* 2011, 115, 6427–6436

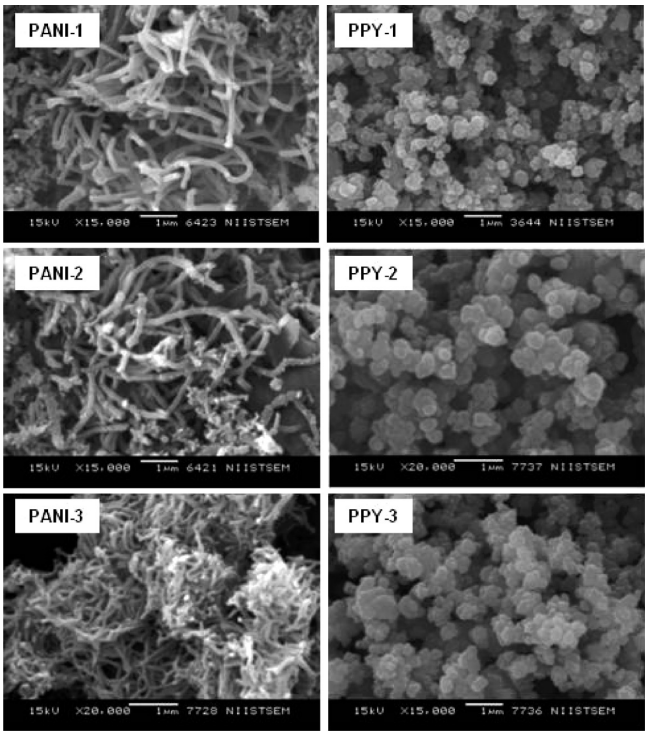

Figure 5. SEM images of homopolymers PANI and PPy.

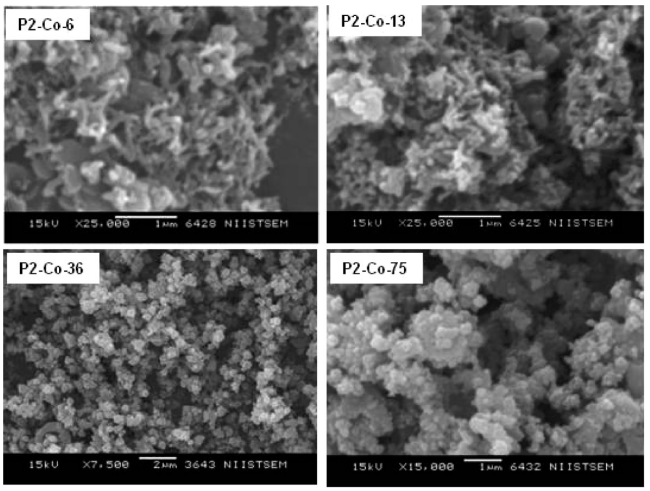

Figure 6. SEM images of copolymers synthesized using dopant-2.

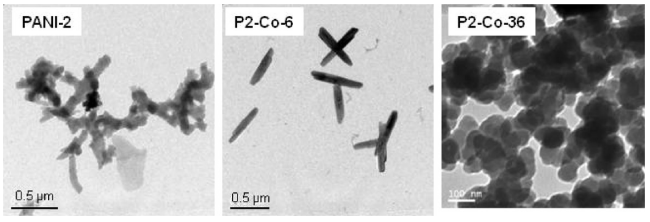

Figure 7. TEM images of the copolymer nanomaterials synthesized using dopant-2.

were assigned at 1300, 1148, and 820 cm^{-1} to C−N stretching of the secondary amine group, O═S═O stretching of the sulfonic acid dopant, and C−H in the 1,4-disubstituted benzene ring out-of-plane stretching, respectively. A weak band at 1714 cm^{-1} in the polypyrrole is assigned to C═O, which arises from the hydroxyl functionality introduced by the nucleophilic attack of water and the subsequent conversion of carbonyl by keto−enol tautomerism.[41] The peaks at 1550, 1195, 1040, 965, and 923 cm^{-1} are assigned to C═C stretching in pyrrole, breathing vibration of the pyrrole rings, N−H (or C−H) in-plane deformation vibration, C−C out-of-ring deformation, and C−H out-of-plane deformation vibrations, respectively.[30,31] The polymerization of both aniline and pyrrole follows the oxidative step-condensation route as in the case of the present approach. Both monomers are oxidized to form aryl radical, which attacks on either the same or other monomer to produce homo or hetero chain linkages. The monomer reactivity of the aniline and pyrrole was reported as r_{An} = 0.13 and r_{py} = 2.16.[33] Therefore, the poly(pyrrole−aniline) copolymers were expected to possess high pyrrole content in the copolymers as compared to that of aniline units, and the random copolymers may have blocky structure.[33] It is very interesting to note that with increase in the amount of aniline in the feed, the peaks at 1580, 1490, 1300, 1148, and 820 cm^{-1} were increasing (move downward) and attained the value of homopolymer, polyaniline. Similarly, the polypyrrole peaks at 1714, 1550, 1195, 1040, 965, and 923 cm^{-1} also increased with the amount of pyrrole in the feed (move upward). The increase in the intensity of the FT-IR peaks with respect to aniline or pyrrole units in the copolymer with increase in their amount of monomer feed confirmed the formation of the expected random copolymer structure. If the copolymer is the mixture of two interpenetrating homopolymers such as polyaniline and polypyrrole rather than the statistical copolymer, then the FT-IR peaks would not have shown such a uniform variation in their peaks with respect to their monomer incorporation. Hence, FT-IR analysis provides direct evidence for the formation of expected random copolymer poly(aniline-*co*-pyrrole). FT-IR spectra of the copolymers synthesized using dopant-2 also showed similar peaks, confirming the copolymer formation (see Figure 6 in the Supporting Information). Thermal stability of the nanomaterials was determined by TGA, and thermograms are provided as Supporting Information. The copolymer nanomaterials have shown high thermal stability, and only 10% weight loss was observed at temperature lower than 280 °C. Azo benzenesulphonic acid-doped polyaniline and copolymer nanomaterials were thermally stable as reported for other dopants such as camphorsulphonic acid.[16]

The morphology of the nanostructures was recorded using scanning electron microscopy (SEM), and the images are shown in Figure 5. The morphology of **PANI-1** and **PANI-2** showed a mat of thick and long nanofibers of length up to 4−6 μm and width of about 200 nm, whereas **PANI-3** produced nanofibers of width 50 nm and length up to 3−5 μm. Polypyrrole samples **PPy-1**, **PPy-2**, and **PPy-3** were nanospheres of size 280 ± 50 nm. SEM images of the copolymer nanomaterials synthesized using dopant-2 are shown in Figure 6. Copolymer samples **P2−Co-6** and **P2−Co-13** have shown the presence of rodlike nanostructures with length of 500−700 nm and width 100−120 nm, whereas **P2−Co-36** and **P2−Co-75** were nanospheres. SEM images of the **P1−Co-*X*** and **P3−Co-*X*** series also showed similar transformation of morphology from nanofibers to nanorod to nanospheres (see the Supporting Information). TEM images (see Figure 7) of the samples **P2−Co-*Y*** and **P1−Co-*Y*** were recorded to provide information about the interior features

dx.doi.org/10.1021/jp2015726 |*J. Phys. Chem. B* 2011, 115, 6427–6436

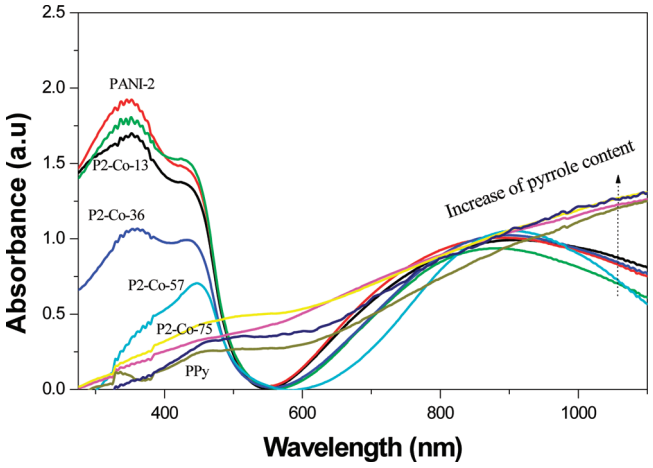

Figure 8. UV−visible spectra of the copolymer synthesized using dopant-2.

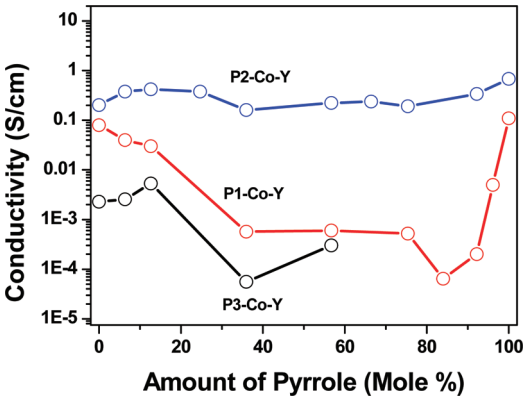

Figure 9. Conductivity of copolymer nanomaterial synthesized with different dopants plotted with amount of pyrrole in feed.

of the nanomaterials (also see the Supporting Information). **PANI-2** showed thick solid nanofibers, whereas **P2−Co-6** and **P2−Co-36** were solid nanorods and nanospheres, respectively. TEM images clearly confirm the formation of solid nanomaterials without any hollow space. Dimensions of the nanostructures calculated from TEM and SEM are relatively in good agreement. Thus, electron microscopic studies clearly reveal that copolymer nanomaterials produce similar morphology transformation for all three anionic dopant-mediated emulsion polymerization routes. In the emulsion polymerization route, the size and shape of the nanostructures were highly dependent on their micellar state, and these micelles either in isolated or aggregated state determined the structures of the resultant nanomaterials. The mechanism for formation of polyaniline nanofiber and polypyrrole nanospheres in the case of homopolymerization is similar to that of our earlier report.[30,31] Dopants produce cylindrical and spherical micellar aggregates with aniline and pyrrole, respectively, which are known to template for fibers and spheres, respectively. In the case of the copolymers, the cylindrical to spherical aggregated transformation occurs in the presence of aniline and pyrrole, which produce nanorods for 5−10% pyrrole in the feed. Interestingly, in the present investigation, all three dopants induce similar morphology transformation in the poly(aniline-*co*-pyrrole).

Absorbance spectra of copolymer and homopolymer nanomaterials were recorded by dispersing the nanomaterials in water; see Figure 8. Amphiphilic nature of the dopants enhances the dispersion stability of the nanomaterials in water. Polyaniline has shown three transitions at 350, 430, and a broad peak at 850 nm with respect to the $\pi-\pi^*$ transition, polaron to conducting band, and valence band to polaron band, respectively.[42−44] Copolymers with higher pyrrole content have shown characteristic peaks corresponding to antibipolaron at 480 nm, and free carrier tail (bipolaron band) at 1000 nm in the NIR region corresponding to polypyrrole chains.[31] The peaks at 380−400 nm were due to the polaron to conduction band of PANI, and the band over 900 nm corresponds to the bipolaron band of polypyrrole. In the present case, we have varied the composition of aniline with pyrrole systematically in the feed, and, therefore, polypyrrole absorption characteristics were dominated at a higher amount of pyrrole in the feed. The decrease in the peak intensity at 380−400 and increase in the peak intensity above 900 nm with increase in the amount of pyrrole in the copolymer confirm the formation of expected random copolymers. The absorbance characteristics were almost unaltered above 35% pyrrole, which suggests that copolymers are saturated with the polypyrrole characteristics above 35%. If the copolymer sample is just the physical mixture of polyaniline and polypyrrole rather than the random incorporation of aniline and pyrrole units in the chain, then one would expect the absorbance spectra of the copolymers may contain the features of both homopolymers. Interestingly, the copolymers showed a uniform variation in the change in the absorbance characteristics (see Figure 8) with increase in the pyrole content in the feed. This trend is almost identical to that of the observation in the FT-IR analysis, which suggests the formation of typical random copolymers rather than statistical or a mixture of homopolymer chains. The absorption changes of other copolymer series were similar with an increase in the amount of pyrrole content (see the Supporting Information).

Copolymer nanomaterials were subjected to conductivity measurement via the four-probe method using Kethley's current and nanovoltmeter source. Electrical conductivity was plotted with percentage feed of pyrrole (mole fraction) for all three series of copolymers shown in Figure 9. The conductivities data for dopant-1 series of copolymers were adapted from earlier reports.[31b] Polyaniline nanofibers **PANI-1**, **PANI-2**, and **PANI-3** showed conductivities in the range of 10^{-2}, 10^{-1}, and 10^{-3} S/cm, respectively. Similarly, the polypyrrole nanospheres **PPy-1** and **PPy-2** showed good conductivity in the rage of their polyaniline counterparts. The conductivities of aniline-rich copolymers (up to 15% of pyrrole in the feed) were almost identical to that of their homoploymers. However, at higher pyrrole content, the conductivity behavior of the copolymers showed a large variation. With increase in pyrrole content (above 30% pyrrole), conductivity was drastically reduced by almost 3 orders of magnitude in the dopant-1 and dopant-3 series. The plots passed through a minimum at 40−60% of pyrole in the feed and subsequently increased to the homo polypyrrole. The data for copolymer series-3 for more than 50% pyrrole were not available due to synthetic limitation. However, the dopant-3 series also showed decreasing trend as observed in the dopant-1 series. Surprisingly, the dopant-2 series did not show any variation in the conductivities, and the plot was found almost linear with values in the order of 10^{-1} S/cm. Stejskal et al. and Lim et al. reported similar nonlinear trend in the conductivity of poly(aniline-*co*-pyrole) samples, which were syntheziesd using HCl as dopants

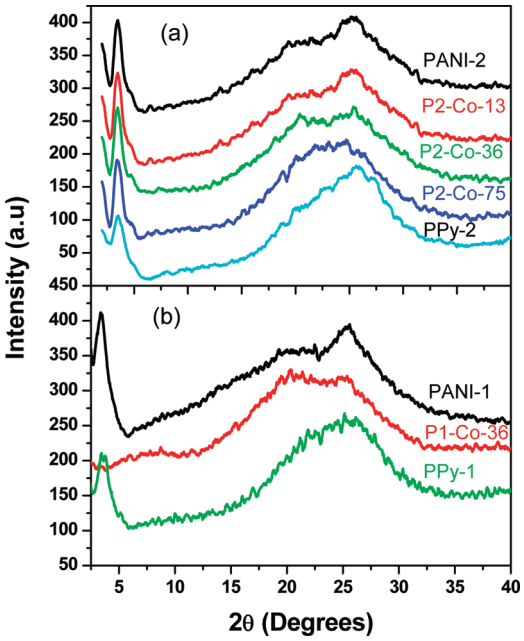

Figure 10. (a) WXRD spectra of the **PANI-2**, **PPY-2**, and copolymers of the **P2**−**Co-*Y*** series. (b) WXRD spectra of the **PANI-1**, **PPY-1**, and **P1**−**Co-36**.

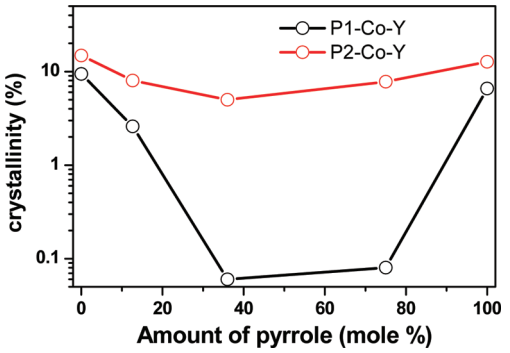

Figure 11. Percentage crystallinity of the copolymer nanomaterials. The values were obtained from the WXRD spectra by deconvoluting method with the variation of ±0.5%.

(but they were not nanomaterials and there was no evidence on morphology transformation).[32,33] Their conductivity plot trend was almost similar to that of dopant-1 (also dopant-3 series) observed in the present investigation. They had attributed the decrease in conductivity of copolymer with increase in pyrrole to the shortening effect of polyaniline chain through the copolymerization or heterodiads formation of aniline with pyrrole rather than to forming aniline blocks. In the present case, it is very difficult to attribute the similar heterodiads formation as reported by the pervious workers[32,33] mainly because the dopant-2 copolymer series did not show any nonlinear conductivity trend despite that they were also synthesized under synthetic conditions identical to those of the dopant-1 and dopant-3 series. Therefore, the nonlinear trend in the conductivity behaviors over the pyrrole composition is not due to the variation in the pyrrole−aniline chemical repeating unit's structure and may be due to other parameters of nanomaterials. The unusual nonlinear conductivity behaviors in the copolymers materials could arise due to two reasons: (i) variation in the morphology of the samples or (ii) difference in the three-dimensional solid-state ordering. Electron microscopic analysis revealed that all three copolymer series showed similar morphological transition from polyaniline fibers to polypyrrole nanospheres via nanorods. Additionally, all three copolymer series were prepared under identical conditions for the same monomer-to-dopant ratio via emulsion polymerization route. Therefore, one could categorically eliminate the influences of morphological transformation on the nonlinear conductivity trends of the copolymers observed in Figure 9.

The solid-state properties of copolymer series-1 and series-2 nanomaterials were studied by wide-angle X-ray diffraction (WXRD) method. Poly(aniline-*co*-pyrrole) copolymers are highly rigid because of their linear structure and less flexible chain. Anionic amphiphilic dopant can induce electrostatic interaction with polymer chain, which organizes the polymer chains in three-dimensional highly ordered fashions. WXRD of copolymer synthesized using dopant-1 and dopant-2 was shown in Figure 10. **PANI-1** showed three peeks at 2θ = 3.5, 19.5, and 25.4 with respect to *d* spacing = 25.5, 4.5, 3.5, respectively. Lower angle peaks of polyaniline were very sharp, and it is attributed to lamellar packing of dopant between polymer chains.[45−50] The higher angle peaks were broad due to diffraction from the aromatic rings and chain−chain interaction of polymer. The homopolymers **PANI-1** and **PPy-1** showed a sharp low angle peak; however, the copolymers **P1**−**Co-36** did not show any lamellar peaks (other copolymers also did not show any low angle peaks; see the Supporting Information). On the other hand, **PANI-2**, **PPY-2**, and their copolymers such as **P2**−**Co-13**, **P2**−**Co-36**, and **P2**−**Co-75** synthesized using double tailed dopant-2 showed both lower angle peaks (corresponding to the lamellar arrangement) as well as higher angle peaks. Thus, a very good solid-state packing is attained in the copolymers of the double tail dopant series as compared to their single tail counterparts. During the emulsion polymerization process, the anionic dopant molecules are permanently attached on the positively charged nanostructures via electrostatic attraction. Because both dopants have identical polar anionic heads, the difference in the observed solid-state ordering among the polymer samples is the result of the variation in the dopant interdigitation tendency in the polymer matrix. Energy minimized structures of the dopants were obtained via the MM2 program using the Chem Draw 8.2 program (see Figure 13 in the Supporting Information; the structures are used to visualize the molecule in three dimensions, which is routinely accepted for fundamental understanding). On the basis of the molecular skeletons of the dopants, a schematic diagram for the interdigitations of the double and single tail dopants is given in the Supporting Information (see Figure 14 in the Supporting Information). The double tail dopant (dopant-2) has long alkyl units spread in a V-shaped geometry, which may provide more possibility for better interdigitations in the polymer chains as compared to that of the dopant-1. To further understand the molecular interaction and packing of the dopants in the solid state, the dopants were subjected to differential scanning calorimeter analysis (see Figure 15 in the Supporting Information). Unfortunately, the DSC plots of dopants (also polymers) did not show any melting or crystallization peaks, and they were found to decompose before melting. All attempts to grow single crystal for the dopant were not successful so far (dopants were found sluggish to crystallize due to limited solubility), and our efforts are continuing to obtain a good

crystal, which may in the future provide more information on the molecular packing.

To quantify the amount of crystallinity in the copolymer series, the amorphous and crystalline peaks were deconvoluted, and the area of crystalline/crystalline + amorphous (% crystallinity) was plotted versus mole feed of pyrrole. In both cases, the homopolymer nanomaterials showed crystallinity ~10%. The values were obtained from the WXRD spectra by deconvoluting method with the variation of ±0.5% crystallinity. Crystallinity of the dopant-1 series decreases with increase in pyrrole content, reaches a minimum, and then increases. This behavior is almost identical to that of their bulk conductivity in Figure 9. However, in the dopant-2 series, the percent crystallinity of the samples remains the same without any loss in the conductivity. This is evident in that the double tail dopant-2 induced stronger lamellar packing via interdigitations in the polymer matrix as compared to that of their single tail counterparts. The stronger interaction between polymer and dopant results in the higher percentage crystallinity of the samples. On the basis of the percentage crystallinity trend in Figure 11 and conductivity plots in Figure 9, it can be directly correlated that the nonlinear trend in conductivity of the copolymer nanomaterials over pyrrole composition was strongly influenced by the solid-state packing of the nanomaterial rather than other parameters, like morphology or repeating unit structure as reported earlier.[31,32] Highly ordered chains enhance the mobility of charge carriers and in turn enhance the bulk conductivity of the conducting polymer nanomaterials. In a nutshell, in the present investigation, we have clearly proved that the design of the surfactant-cum-dopant is very crucial factor in developing highly order, highly conducting, and good morphology conducting polymers and correlating their structure−property relationships, exclusively poly(aniline-*co*-pyrrole) copolymers.

CONCLUSION

Three anionic amphiphilic dopants having identical polar heads and different hydrophobic tails have been designed and synthesized to understand the structure property relationships of poly(aniline-*co*-pyrrole) nanomaterials. Important outcomes of the present approaches were as follows: (i) Amphiphilic anionic dopants were synthesized by the diazotization reaction of cardanol and phenol and utilize the resultant molecules as structure-directing agent-cum dopant for conducting polymer nanomaterials, (ii) the amphiphilies produce 4.3 and 100 nm micelles in water depending upon their hydrophobic tail nature, (iii) dopant micelles form stable emulsion with aniline, pyrrole, and their monomer mixtures, which facilitate synthesis of copolymer nanomaterials via emulsion polymerization route, (iv) morphology of the copolymer nanomaterials was found to undergo transformation from nanofibers through nanorods to nanospheres, (v) copolymer nanomaterials synthesized using single tail (or no tial) amphiphiles showed nonlinear trend in their four-probe bulk conductivity over the pyrrole content in the copolymer, (vi) copolymers obtained using double tail amphiphilies followed a linear bulk conductivity trend over the entire copolymer composition, (vii) based on the electron microscopic analysis, the effect of the morphological transformation on the nonlinear trend in the conductivity of the copolymers was ruled out, (viii) WXRD analysis of copolymer nanomaterials reveals that copolymers synthesized using double tailed dopant are packed via lamellar chains and hence possessed long-range order in the copolymer matrix, (xi) WXRD analysis produces direct evidence that solid-state ordering of the nanostructures plays a major role in the conductivity of the nanomaterials rather than morphology transformation, and (x) the structures of the amphiphilies are a crucial factor in determining the solid-state ordering, conductivity, and morphology, and, in the present case, double tail dopants are found to be superior in controlling the properties of the copolymer nanomaterial, more specifically, poly(aniline-*co*-pyrrole).

ASSOCIATED CONTENT

Supporting Information. ^{13}C spectra and FT-IR of the dopants, DLS histogram of the copolymers, ^{1}H NMR and FT-IR spectra of the nanomaterials, TGA profile of the nanomaterials, TEM and SEM images of the nanomaterials, photographs of the emulsion mixture before polymerization, and UV−visible spectra of nanomaterials. This material is available free of charge via the Internet at http://pubs.acs.org.

AUTHOR INFORMATION

Corresponding Author

*Fax: +91-20-2589 9790. E-mail: jayakannan@iiserpune.ac.in.

ACKNOWLEDGMENT

We thank the Department of Science of Technology, New Delhi, India, for financial support under the NSTI Programme-SR/S5/NM-06/2007 and SR-NM/NS-42/2009 schemes. We thank Dr. Peter Koshy, M. R. Chandran, Dr. V. S. Prasad, Mr. Robert Philip, Dr. U. Syamaprasa, and Mr. P. Guruswamy for SEM, TEM, and WXRD analysis, NIIST-Trivandrum. M.J.A. thanks UGC-New Delhi, India, for a Senior Research Fellowship (SRF).

REFERENCES

(1) Huang, J.; Virji, S.; Weiller, B. H.; Kaner, R. B. *J. Am. Chem. Soc.* **2003**, *125*, 314.
(2) Huang, J.; Virji, S.; Weiller, B. H.; Kaner, R. B. *Chem.-Eur. J.* **2004**, *10*, 1314.
(3) Cosnier, S. *Electroanalysis* **2005**, *17*, 1701.
(4) Leclerc, M. *Adv. Mater.* **1999**, *11*, 1491.
(5) Ko, S.; Jang, J. *Biomacromolecules* **2007**, *8*, 182.
(6) Janata, J.; Josowich, M. *Nat. Mater.* **2003**, *2*, 19.
(7) Jang, J. *Adv. Polym. Sci.* **2006**, *199*, 189.
(8) Jang, J.; Yoon, H. *Small* **2005**, *1*, 1195.
(9) Gerard, M.; Chaubey, A.; Malhotra, B. D. *Biosens. Bioelectron.* **2002**, *17*, 345.
(10) Geetha, S.; Rao, C. R. K.; Vijayan, M.; Trivedi, D. C. *Anal. Chim. Acta* **2006**, *568*, 119.
(11) Wu, A.; Kolla, H.; Manohar, S. K. *Macromolecules* **2005**, *38*, 7873.
(12) Jang, J.; Oh, J. H.; Stucky, G. D. *Angew. Chem., Int. Ed.* **2002**, *41*, 4016.
(13) Zhong, W.; Liu, S.; Chen, X.; Wang, Y.; Yang, W. *Macromolecules* **2006**, *39*, 3224.
(14) Zhang, X.; Manohar, S. K. *Chem. Commun.* **2004**, 2360.
(15) DeArmitt, C.; Armes, S. P. *Langmuir* **1993**, *9*, 652.
(16) (a) Shen, Y.; Wan, M. *Synth. Met.* **1998**, *96*, 127. (b) Omastova, M.; Trchova, M.; Kovarova, J.; Stejskal, J. *Synth. Met.* **2003**, *138*, 447.
(17) Haung, K.; Wan, M.; Long, Y.; Chen, Z.; Wei, Y. *Synth. Met.* **2005**, *155*, 495.

(18) Bay, L.; Mogensen, N.; Skaarup, S.; Sommer-larsen, P.; Jorgenson, M.; West, K. *Macromolecules* **2002**, *35*, 9345.
(19) Liu, L.; Zhao, C.; Zhao, Y.; Jia, N.; Zhuo, Q.; Yan, M.; Jiang, Z. *Eur. Polym. J.* **2005**, *41*, 2117.
(20) Menon, V. P.; Lei, J.; Martin, C. R. *Chem. Mater.* **1996**, *8*, 2382.
(21) Ikegame, M.; Tajima, K.; Aida, T. *Angew. Chem., Int. Ed.* **2003**, *42*, 2154.
(22) Zhang, X.; Zhang, J.; Song, W.; Liu, Z. *J. Phys. Chem. B* **2006**, *110*, 1158.
(23) Stejskal, J.; Omastova, M.; Fedorova, S.; Prokes, J.; Trchova, M. *Polymer* **2003**, *44*, 1353.
(24) He, C.; Yang, C.; Li, Y. *Synth. Met.* **2003**, *139*, 539.
(25) Liu, J.; Wan, M. *J. Mater. Chem.* **2001**, *11*, 404.
(26) Zhang, L.; Wan, M. *Thin Solid Films* **2005**, *447*, 24.
(27) Jang, J.; Yoon, H. *Langmuir* **2005**, *21*, 11484.
(28) Jang, J.; Yoon, H. *Chem. Commun.* **2003**, 720.
(29) Virji, S.; Kaner, R. B.; Weiller, B, H. *J. Phys. Chem. B* **2006**, *110*, 22266.
(30) (a) Anilkumar, P.; Jayakannan, M. *Langmuir* **2006**, *22*, 5952. (b) Anilkumar, P.; Jayakannan, M. *J. Phys. Chem. C* **2007**, *111*, 3591. (c) Anillkumar, P.; Jayakannan, M. *Macromolecules* **2007**, *40*, 7311. (d) Anillkumar, P.; Jayakannan, M. *Macromolecules* **2008**, *41*, 7706. (e) Anilkumar, P.; Jayakannan, M. *J. Phys. Chem. B* **2009**, *113*, 11614. (f) Anilkumar, P.; Jayakannan, M. *J. Phys. Chem. B* **2010**, *114*, 728. (g) Anilkumar, P.; Jayakannan, M. *J. Appl. Polym. Sci.* **2009**, *114*, 3531–3541.
(31) (a) Antony, M. J.; Jayakannan, M. *J. Phys. Chem. B* **2007**, *111*, 12772. (b) Antony, M. J.; Jayakannan, M. *J. Polym. Sci., Part B: Polym. Phys.* **2009**, *47*, 830. (c) Antony, M. J.; Jayakannan, M. *J. Phys. Chem. B* **2010**, *114*, 1314.
(32) Stejskal, J.; Trchova, M.; Ananieva, I. R.; Janca, J.; Prokes, J.; Fedorov, S.; Sapurina, I. *Synth. Met.* **2004**, *146*, 29.
(33) Lim, V. W. L.; Kang, E. T.; Neoh, K. G.; Ma, Z. H.; Tan, K. L. *Appl. Surf. Sci.* **2001**, *181*, 317.
(34) Sari, M.; Talu *Synth. Met.* **1998**, *94*, 221.
(35) Fusalba, F.; Ḃelanger, D. *J. Phys. Chem. B* **1999**, *103*, 9044.
(36) Li, X.; Zhang, X.; Li, H. *J. Appl. Polym. Sci.* **2001**, *81*, 3002.
(37) Kim, J. W.; Cho, C. H.; Liu, F.; Choi, H. J.; Joo *J. Synth. Met.* **2003**, *17*, 135.
(38) Cho, C. H.; Choi, H. J.; Kim, J. W.; Jhon, M. S. *J. Mater. Sci.* **2004**, *39*, 1883.
(39) (a) Zhou, C.; Han, J.; Song, G.; Guo, R. *J. Polym. Sci., Part A: Polym. Chem.* **2008**, *46*, 3563. (b) Li, X. G.; Wnag, L. X.; Zhu, Z. L.; Yang, Y. L. *J. Appl. Polym. Sci.* **2001**, *82*, 510. (c) Li, X. G.; Haung, M. R.; Wang, L. W.; Zhu, M. F.; Menner, A.; Springer, J. *Synth. Met.* **2001**, *123*, 435. (d) Li, X. G.; Chen, R. F.; Haung, M. R.; Zhu, M. F.; Chen, Q. *J. Polym. Sci., Part A: Polym. Chem.* **2004**, *42*, 2073.
(40) Ping, Z. *J. Chem. Soc., Faraday Trans.* **1996**, *92*, 3063.
(41) Christensen, P. A.; Hamnet, A. *Electrochim. Acta* **1991**, *36*, 1263.
(42) MacDiarmid, A. G.; Zhou, Y.; Feng, J. *Synth. Met.* **1999**, *100*, 131.
(43) Cabala, R.; Skarda, J.; Potje-Kamloth, K. *Phys. Chem. Chem. Phys.* **2002**, *2*, 3283.
(44) Xia, Y.; Wiesinger, J. M.; MacDiarid, A. G. *Chem. Mater.* **1995**, *7*, 443.
(45) Jayakannan, M.; Annu, S.; Ramalekshmi, S. *J. Polym. Sci., Part B: Polym. Phys.* **2005**, *43*, 1321.
(46) Jana, T.; Nandi, A. K. *Langmuir* **2000**, *16*, 3141.
(47) Jana, T.; Nandi, A. K. *Langmuir* **2001**, *17*, 5768–5774.
(48) Jana, T.; Chatterjee, J.; Nandi, A. K. *Langmuir* **2002**, *18*, 5720.
(49) Song, M. K.; Kim, Y. T.; Kim, B. S.; Kim, J.; Char, K.; Rhee, H. W. *Synth. Met.* **2004**, *141*, 315.
(50) Wernet, W.; Monkenbusch, M.; Wegner, G. *Macromol. Chem. Rapid Commun.* **1984**, *5*, 157.